# Photodissociation of $H_2^+$ in intense chirped laser fields

J. T. Lin
*National Center for Theoretical Sciences, Physics Division, P.O. Box 2-131, Hsinchu 30013, Taiwan*

T. F. Jiang
*Institute of Physics, National Chiao Tung University, 1001 Ta-Hsueh Road, Hsinchu 30010, Taiwan*

(Received 10 July 2000; revised manuscript received 25 August 2000; published 8 December 2000)

Regarding an experimental measurement of proton kinetic energy spectra of $H_2^+$ with a chirped pulse [L. J. Frasinski, J. H. Posthumus, J. Plumridge, and K. Colding, Phys. Rev. Lett. **83**, 3625 (1999)], we present a nonperturbative, time-dependent calculation for the photodissociation of $H_2^+$ in intense laser fields by combining three numerical techniques. The results show a finer kinetic-energy distribution structure of a proton due to the intrapulse pump-dump mechanism between two electronic states as the pulse duration and intensity change. Higher-energy peaks are also suppressed by frequency chirping of the laser field. The dissociation probabilities show that a positively chirped pulse is always more efficient for population inversion than no chirping or negatively chirped pulses, and a slight coordinate shift of the initial state could result in a significant increase of dissociation probability.

DOI: 10.1103/PhysRevA.63.013408 PACS number(s): 42.50.Hz, 33.80.Gj, 33.80.Wz

## I. INTRODUCTION

Molecular dissociation in strong laser fields has been actively investigated in the past few years, both experimentally and theoretically. At intensities above 10 TW/cm$^2$, atoms exhibit multiphoton ionization (MPI) and above-threshold ionization (ATI), where they absorb more photons than the minimum requirement to ionize [2]. Molecules have additional rotational and vibrational degrees of freedom that lead to other interesting phenomena as well as ATI, such as dissociative ionization, above-threshold dissociation (ATD), bond softening and hardening, etc. [3–12]. For ATD, the internuclear electronic potentials are mixed by the laser field at points of multiphoton resonance, causing the molecules to dissociate via several possible channels corresponding to the absorption of one, two, or more photons. A closely related phenomenon is bond softening, where the potential curves flattened or ''softened'' in the vicinity of a multiphoton resonance. And bond hardening occurs when the molecules are trapped in the dressed potential curves [1,4–6].

On the other hand, laser control of quantum systems is one of the interesting themes of modern atomic and molecular physics. The use of chirped pulses has been demonstrated to be a possible method of efficient vibrational ladder climbing within a single pulse both experimentally and theoretically [13–15]. Because the frequency sweeps in time, the chirped pulse could be tailored to match the anharmonicity of vibrational energy levels during the excitation process. But there have been only a few studies done on the chirping transition between different electronic states of molecules. Cao *et al.* [16] showed the robustness of population inversion of LiH electronic states under positive chirped pulses where frequency varying becomes off resonance with the wave packet moving downward on the potential curve. Meyer *et al.* [17] proposed that by using a second chirped probe pulse, the motion of the wave packet can be distinguished by the appropriately chirped electric field. Frasinski *et al.* reported the first experiment of bond hardening by using 100-200 TW/cm$^2$ femtosecond chirped pulses of 792 nm [1]. They explored the dynamics of an ion trap during the dissociation process and found that the released proton kinetic energy depends on the speed of the intensity decrease. They also used chirped pulses to test if the wavelength variation affects the one-photon peak in the leading and trailing edges of the pulse. Their results revealed that the proton kinetic-energy spectra (PKES) are symmetric in positive and negative chirping, and that the dynamics of the bond hardening is independent of the chirping direction.

Although $H_2^+$ is the simplest molecule, under strong laser fields it still shows surprisingly complicated phenomena and reveals rich dynamical characteristics that are absent in the atomic equivalent. Therefore, it is worthwhile to choose $H_2^+$ for the study of dissociation dynamics from the fragment kinetic-energy spectra because of its simplicity and its potential for rich insight. In this paper, we apply the splitting wave method [18,19] to the $H_2^+$ $^2\Sigma_g$ and $^2\Sigma_u$ states by using the Pauli matrices [20], which allows us to extract PKES from the asymptotic region and avoid the boundary problem. The rotational degrees of freedom will be neglected without losing physical insight within these field parameters [4,16]. The paper is organized as follows. The numerical methods are described in Sec. II, where these methods are readily applied to more than two-levels systems. In Sec. III, computational results of various laser-field parameters are presented. The PKES are investigated for different intensities, pulse durations, and chirping parameters. The influence of initial states on dissociation dynamics by shifting the wave function in spatial and momentum coordinates is also explored therein. Finally, a conclusion is given in Sec. IV.

## II. THEORY

We assume that only two charge-resonant electronic states ($^2\Sigma_g$,$^2\Sigma_u$) are coupled by the laser field $E(t)$ within the Born-Oppenheimer approximation. The equations de-

 

scribing the nuclear motion of a diatomic molecule interacting with the laser pulse are

$$i\hbar\frac{\partial\psi_j(R,t)}{\partial t}=-\frac{\hbar^2}{2\mu}\frac{\partial^2\psi_j(R,t)}{\partial R^2}+V_j(R)\psi_j(R,t)-\mu_{12}(R)E(t)\psi_k(R,t), \quad (1)$$

where $j,k=1,2$ and $j\neq k$. The ground-state (excited-state) wave function is $\psi_1(R,t)$ $[\psi_2(R,t)]$, which describes the nuclear motion of the molecule in the ground (excited) electronic state potential curve $V_1(R)$ $[V_2(R)]$. $\mu_{12}(R)$ is the transition dipole moment and $\mu$ is the reduced mass of the system.

### A. Time propagation and space splitting

In this section, we briefly describe how to calculate the time propagation of the two-state wave functions by using the split operator (SPO) method with fast Fourier transform (FFT) [21,22]. It is straightforward to extend this method to cases of more than two states with the generalized Pauli matrix [20]. The Schrödinger equation to be solved is of the form (atomic units are used throughout, unless otherwise stated)

$$i\frac{\partial}{\partial t}\begin{pmatrix}\psi_1(R,t)\\ \psi_2(R,t)\end{pmatrix}=\begin{pmatrix}H_1 & \mu_{12}(R)\\ \mu_{12}(R) & H_2\end{pmatrix}\begin{pmatrix}\psi_1(R,t)\\ \psi_2(R,t)\end{pmatrix}. \quad (2)$$

Here, $H_i(=K_i+V_i)$ is the Hamiltonian consisting of the kinetic operator $T_i$ and the potential-energy operator $V_i$ for the $i$th electronic state. In the SPO method, the formula for time evolution of a total wave function from time $t$ to $t+\Delta t$ is expressed as follows:

$$\Psi(t+\Delta t)\approx \exp[-i\hat{K}\Delta t/2]\exp[-i\hat{V}_o\Delta t/2]\exp[-i\hat{V}_d\Delta t]\times\exp[-i\hat{V}_o\Delta t/2]\exp[-i\hat{K}\Delta t/2]\Psi(t), \quad (3)$$

where $\hat{V}_d$ and $\hat{V}_o$ are the diagonal and off-diagonal matrix, respectively,

$$\hat{V}_d=\begin{pmatrix}V_1(R) & 0\\ 0 & V_2(R)\end{pmatrix},$$

$$\hat{V}_o=\begin{pmatrix}0 & \mu_{12}(R)E(t)\\ \mu_{12}(R)E(t) & 0\end{pmatrix}. \quad (4)$$

Using the identity $\exp[-i\sigma_x\theta/2]=\mathbf{1}\cos(\theta/2)-i\sigma_x\sin(\theta/2)$, where $\sigma_x=\left(\begin{smallmatrix}0&1\\1&0\end{smallmatrix}\right)$ and $\mathbf{1}$ is the identity matrix, the propagation becomes

$$\Psi(t+\Delta t)\approx \exp[-i\hat{K}\Delta t/2]\hat{Z}(R,t)\exp[-i\hat{V}_d\Delta t]\times\hat{Z}(R,t)\exp[-i\hat{K}\Delta t/2]\Psi(t), \quad (5)$$

with

$$\hat{Z}(R,t)=\mathbf{1}\cos[\mu_{12}(R)E(t)\Delta t/2]-i\sigma_x\sin[\mu_{12}(R)E(t)\Delta t/2],$$

which is a unitary operator and will preserve the wave-function norm. By substituting the generalized Pauli matrix for the Pauli matrix in the $\exp[-i\hat{V}_o\Delta t/2]$ expansion, the extension of this method to more than two states is straightforward.

Although the SPO method is very efficient with FFT, there is a troublesome boundary problem due to the spreading of the wave function under the stretching of an external field. This would make the calculation time-consuming, as the grid points would have to be increased to a large number to compensate. To avoid this difficulty, we divide the grid space into two regions: one is the *asymptotic region* $(A)$, where the nuclei are widely separated and the potential energies $V_j(R)$ are constants, and the other is the *interaction region* $(I)$, where the interaction potential plays a part. The wave functions are split into $\psi_j^I(R,t)$ and $\psi_j^A(R,t)$ by a filter function $f(R)$, which is essentially equal to 1 in the interaction region and decays gradually to zero in the asymptotic region:

$$\psi_j(R,t)=\psi_j^I(R,t)+\psi_j^A(R,t) \quad (6)$$

and

$$\psi_j^I(R,t)=f(R)\psi_j(R,t),\quad \psi_j^A(R,t)=[1-f(R)]\psi_j(R,t). \quad (7)$$

In contrast to the conventional method, which drops the asymptotic wave function and keeps only the interaction region wave function, this technique can maintain the asymptotic wave function without losing the information from the fragmentations [18,19].

### B. Propagation of $\psi_j^A(R,t)$ in momentum space

The linearity of the Schrödinger equation allows us to propagate $\psi_j^I(R,t)$ and $\psi_j^A(R,t)$ separately. For the $H_2^+$ homonuclear molecule, the transition dipole moment diverges as $eR/2$ asymptotically. It enables us to manipulate the wave functions easily in momentum space by Volkov states [23,24] or a plane wave in the asymptotic region, as described below. The coupling equation describing the evolution of the asymptotic wave function is then

$$i\hbar\frac{\partial\psi_j^A(R,t)}{\partial t}=-\frac{\hbar^2}{2\mu}\frac{\partial^2\psi_j^A(R,t)}{\partial R^2}-\frac{eRE(t)}{2}\psi_k^A(R,t), \quad (8)$$

where $j,k=1,2$ and $j\neq k$. This equation can be decoupled by introducing the following new wave function:

$$\chi_j(R,t)=\frac{1}{\sqrt{2}}[\psi_1^A(R,t)\pm\psi_2^A(R,t)],\quad j=1,2 \quad (9)$$

and the time evolution of the new wave function is determined by the following equation:

$$i\hbar\frac{\partial\chi_j(R,t)}{\partial t}=-\frac{\hbar^2}{2\mu}\frac{\partial^2\chi_j(R,t)}{\partial R^2}\mp\frac{eRE(t)}{2}\chi_j(R,t). \tag{10}$$

In the above equation, we can see that the equation of motion is the same for $\chi_1$ and $\chi_2$ other than the sign of the electric field being opposite. Therefore, the following discussion is applicable to either $\chi_1$ or $\chi_2$. Obviously, these equations are formally analogous to the equation of motion of a free electron moving in the electric field $E(t)$. The solutions are the well-known Volkov states. For this reason, it is a good choice to use the Volkov states as the basis set to expand the asymptotic wave function in the momentum space like the Fourier expansion of the motion for a free-particle wave packet. Let $\phi_k(R,t,t_i)$ be the time-dependent Volkov state, which reduces to plane waves at time $t_i$:

$$\phi_k(R,t,t_i)=\exp\{i[k+A(t,t_i)]R\}\times\exp\left[-i\int_{t_i}^{t}dt'\frac{\hbar}{2\mu}[k+A(t,t')]^2\right], \tag{11}$$

where

$$A(t,t_i)=\frac{e}{2\hbar}\int_{t_i}^{t}dt'E(t'). \tag{12}$$

If we know the expansion coefficients $\hat{\chi}_j(k,t_i)$ such that the expression of $\chi_j(R,t_i)$ at time $t_i$ is

$$\chi_j(R,t_i)=\frac{1}{\sqrt{2\pi}}\int dk\,\hat{\chi}_j(k,t_i)\phi_k(R,t_i,t_i), \tag{13}$$

then $\chi_j(R,t)$ $(t\geq t_i)$ is simply determined by the time evolution of the basis set $\{\phi_k(R,t,t_i)\}$:

$$\chi_j(R,t)=\frac{1}{\sqrt{2\pi}}\int dk\hat{\chi}_j(k,t_i)\phi_k(R,t,t_i). \tag{14}$$

Another way of showing this is to propagate the asymptotic wave function in momentum space, thus defining the Fourier transform of $\chi_j(R,t)$ at time $t$:

$$\hat{\chi}_j(k,t)=\frac{1}{\sqrt{2\pi}}\int dR\,\chi_j(R,t)e^{-ikR}. \tag{15}$$

Using Eq. (14) and the definition of $\phi_k(R,t,t_i)$, we obtain

$$\hat{\chi}_j(k,t)=\hat{\chi}_j(k\mp\Delta(t,t_i),t_i)\exp\left[-i\frac{\hbar}{2\mu}\int_{t_i}^{t}dt'[k\mp A(t,t')]^2\right]. \tag{16}$$

We see that the time evolution of the $\hat{\chi}_j(k,t)$ $(j=1,2)$ functions is very simple in the momentum space. To obtain $\hat{\chi}_j(k,t)$ at any time $t\geq t_i$, we just have to shift in $k$ space the initial $\hat{\chi}_j(k,t_i)$ by the laser pulse area and multiply by a phase factor. Finally, the asymptotic wave functions in momentum space can be recovered by using Eq. (9).

## III. NUMERICAL RESULTS AND DISCUSSION

The theory presented in the preceding section will be applied to photodissociation of the $H_2^+$ molecule. It is well known that dissociation fragments of $H_2^+$ reveal multiphoton behavior under intense-field–above-threshold dissociation (ATD), which is observed experimentally for proton kinetic-energy spectra (PKES). As a calibration, we use the method described above and obtain exactly the same energy spectra of proton fragments as Keller did [19]. Classically, the transition frequency varies with nuclear separation distance $R$ of $H_2^+$ when the molecule is driven by the external field and moves on the potential curve. Thus we use a frequency sweeping pulse (chirped pulse) to excite the molecule and study its dissociation and fragment spectrum. Furthermore, since the moving direction of the molecule in the potential could decide the excitation dynamics, we will prepare the initial states of the system at different nuclear separation distance and velocity to investigate their influence on the excitation of the molecule.

### A. Propagation algorithm and the calculation of the PKES

The propagation scheme was discussed in detail in [19] and we just give a brief description here. An initial wave packet is chosen and propagated in the coordinate space, which will be separated into $\psi_j^I(R,t)$ and $\psi_j^A(R,t)$ whenever the wave function $\psi_j^I(R,t)$ accumulates to a small value $\epsilon$ $(\sim 10^{-5})$ at the grid boundary. The asymptotic wave functions are then propagated in the momentum space via a Volkov state basis. During the field-matter interaction, the pulse area $A(t,t')$ has to be calculated as well as its integral. At each moment of the wave-packet splitting, the new asymptotic part of the wave functions is added to the previous ones. The pulse area and its integral are calculated from the previous splitting time $t_i$ to the latest splitting time $t_{i+1}$. It will save the computational time that we do not have to calculate the integrals from $t_i$ to the time pulse turned off at each step, and we can extract the information we need from the wave function at any time during the propagation.

The fragment probability distribution is given by

$$P(k)=\lim_{t\to\infty}[|\hat{\psi}_1^A(k,t)|^2+\hat{\psi}_2^A(k,t)|^2] \tag{17}$$

and the kinetic-energy spectrum can be written as

$$S(E)=\frac{1}{\hbar}\sqrt{\frac{\mu}{2E}}P(\sqrt{2\mu E}/\hbar). \tag{18}$$

We have seen in Sec. II that the propagation of the asymptotic part is done in the momentum space, therefore we obtain directly the needed wave function in $k$ space. Finally, the total photodissociation probability may be obtained by integrating $P(k)$ over $k$:

$$P_d=\int dk\,P(k)=\lim_{t\to\infty}\left(1-\int dR|\psi_1^I(R,t)|^2\right). \tag{19}$$

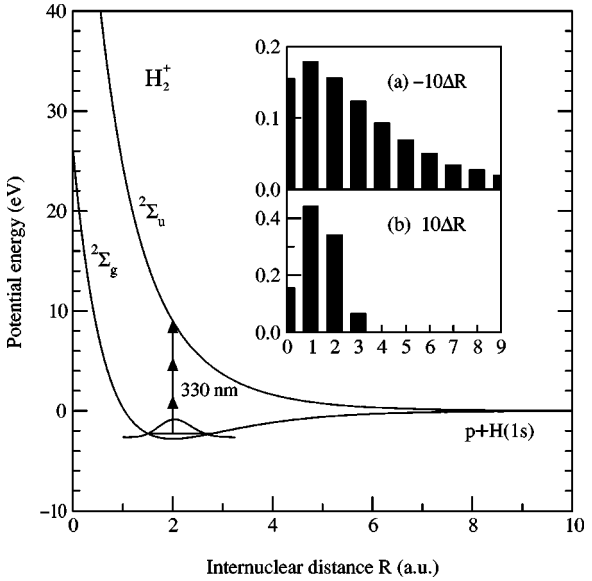


FIG. 1. Simplified potential-energy curves for the electronic ground and excited states of $H_2^+$ with the vibrational ground-state wave function at the bottom of the $^2\Sigma_g$ potential curve. The ground state is excited to the upper electronic state by a 330-nm laser pulse via the multiphoton process. The insets show the vibrational state distributions when the $H_2^+$ ground state is shifted from its equilibrium position by $-10\Delta R$ or $10\Delta R$, where $\Delta R=0.0625$ a.u.

### B. Computational features

The calculations are based on a mesh of 512 grid points extending for $R=0$ to $R_{\max}=32$ a.u. The $H_2^+$ molecule is subject to a Gaussian pulse with an extent of $\sqrt{2\ln 2}\tau$ full width at half maximum (FWHM):

$$E(t)=E_m\exp\left[-\left(\frac{t-4\tau}{\tau}\right)^2\right]\cos(\omega_L t),$$

$$\omega_L=\begin{cases}\omega_0\left(1+\dfrac{\alpha_c t}{8\tau}\right) & \text{for } t\leqslant 8\tau,\\ \omega_0(1+\alpha_c) & \text{for } t>8\tau,\end{cases} \tag{20}$$

where $E_m$ and $\omega_0$ are the peak field strength and laser frequency, respectively. The $\omega_0$ is chosen to be 330 nm and the propagation time step $\Delta t=0.8$ a.u. $\alpha_c$ is the chirping parameter, which specifies the frequency sweeping rate and is positive (negative) if frequency increases (decreases) with time. Figure 1 shows the simplified two-potential-curves diagram of $H_2^+$ excited by a 330-nm laser pulse that is just a little above the dissociation threshold of $H_2^+$ and was used to study the multiphoton dissociation processes and ATD dynamics of this molecular ion by many authors, both experimentally and theoretically [3–7,10,19]. Today most of the pulse chirping is produced in the visible and infrared range by controlling such parameters as the distance between two gratings in the compressor of the optical system [25,26]. It is believed that the chirping of an ultraviolet and soft x ray generated from harmonic up-conversion will not be difficult to achieve in the future [27,28]. To get an idea about the relation between the pulse duration and $\alpha_c$, we follow the derivation presented by Balling *et al.* [25] and compare with Eq. (20) to give some results. As an example, a 300-nm and 5.5-fs bandwidth-limited pulse would be stretched to 100 fs for $\alpha_c=\pm 0.3$, and $\alpha_c=\pm 0.1100$ fs pulses result from a 16.3-fs chirping-free pulse.

The transition dipole moment $\mu(R)$ is fitted to Ref. [29] in the $R\to 0$ and $R\to\infty$ regions,

$$\mu(R)=\frac{R}{2(1-S^2)^{1/2}}-\frac{1}{2+1.4R}, \tag{21}$$

where the overlapping integral $S=e^{-R}(1+R+R^2/3)$. The filter function is taken as

$$f(R)=\{1+\exp[\sigma(R-R_0)]\}^{-2}, \tag{22}$$

where $R_0$ is the point dividing the interaction and the asymptotic regions, and $\sigma$ controls the extension of the transition zone between these two regions. In our calculation, we choose $R_0=0.75R_{\max}$ and $\sigma=120/R_{\max}$.

In our calculation, the initial states are chosen to be the $^2\Sigma_g$ vibrational ground state with its initial velocity and position being shifted by an amount $\langle R\rangle$ and $\langle k\rangle$ from the equilibrium values. To prepare these initial states with different initial velocity and position, we can just multiply the ground state by a phase factor $\exp[i\langle k\rangle R]$ and shift the coordinate of the wave function by $\langle R\rangle$, that is, we can do the following Fourier transform (FT) in the coordinate and momentum dual spaces:

$$\Psi_0(R-\langle R\rangle)\exp[i\langle k\rangle R]\overset{\text{FT}}{\leftrightarrow}\hat{\Psi}_0(k-\langle k\rangle)\exp[-ik\langle R\rangle]. \tag{23}$$

The shifts $\langle R\rangle$ and $\langle k\rangle$ are equal to $m\Delta R$ and $n\Delta k$ with *integers* $(m,n)$, where $\Delta R=0.0625$ a.u. and $\Delta k=0.196\,35$ a.u. are the grid sizes of the coordinate and momentum spaces. This kind of initial state could be produced by applying a dc electric field to the $H_2^+$ molecules. The shifted ground state then consists of several vibrational eigenstates. Under the chirped pulses, the excitation dynamics from each state can be explored.

### C. Dissociation and PKES of $H_2^+$ under chirped pulses

First, we explore the dissociation of $H_2^+$ under pulses from low intensity to high intensity, from negative to positive chirping constants, and from a few femtoseconds (the order of the vibrational period) up to subpicosecond pulse duration. The results are shown in Figs. 2(a)–2(d). In Fig. 2(a), the intensity is 5 TW/cm$^2$. The maximum dissociation probabilities $P_d$ of $H_2^+$ at $\alpha_c=0.3$ are $1.15\times10^{-6}$, $5.28\times10^{-6}$, $5.28\times10^{-5}$, $1.05\times10^{-5}$, $2.63\times10^{-5}$, and $5.26\times10^{-5}$ for pulse durations of 10, 50, 100, 250 and 500 fs, respectively. For visualization purposes, we normalize each curve with $P_d$ at $\alpha_c=0.3$. After the scaling, all results of the five different pulse durations show the same behavior. That is, the dissociation is much more efficient for positive chirping than negative chirping. When the wave packet is excited to the $^2\Sigma_u$ state, it gains momentum and accelerates

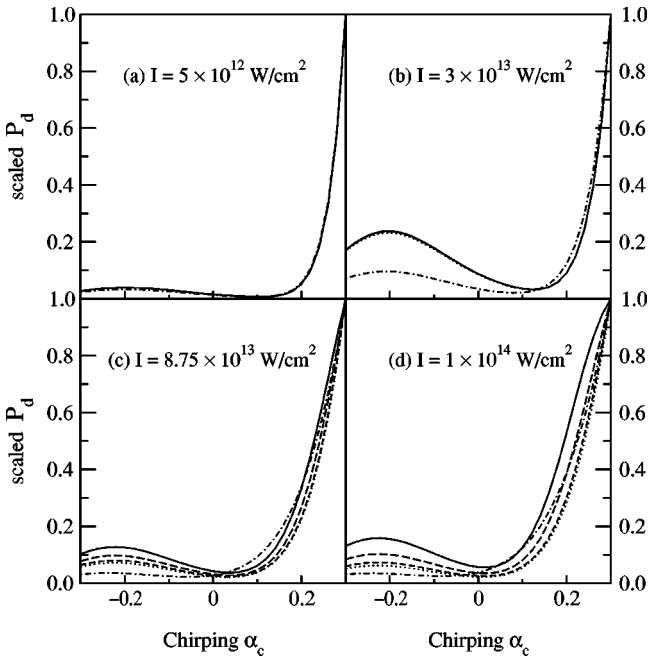


FIG. 2. Dissociation probabilities $P_d$ of $H_2^+$ vs chirping parameter $\alpha_c$ for different pulse intensity and duration $\tau$. Dashed-dotted line: $\tau=10$ fs, dotted line: $\tau=50$ fs, short dashed line: $\tau=100$ fs, long dashed line: $\tau=250$ fs, and solid line: $\tau=500$ fs. All the $P_d$ are scaled by the dissociation probability $P_d$ $(\alpha_c=0.3,\tau)$ in each case. In (a), $P_d$ $(\alpha_c=0.3,\tau=10$ fs$)=1.16\times10^{-6}$, $P_d$ $(\alpha_c=0.3,\tau=50$ fs$)=5.28\times10^{-6}$, $P_d$ $(\alpha_c=0.3,\tau=100$ fs$)=1.05\times10^{-5}$, $P_d$ $(\alpha_c=0.3,\tau=250$ fs$)=2.63\times10^{-5}$, $P_d$ $(\alpha_c=0.3,\tau=500$ fs$)=5.26\times10^{-5}$; (b) $P_d$ $(\alpha_c=0.3)$ are $6.95\times10^{-4}$, $1.39\times10^{-3}$, $2.74\times10^{-3}$, $6.79\times10^{-3}$, and $1.35\times10^{-2}$ for $\tau=10$ fs, 50 fs, 100 fs, 250 fs and 500 fs, respectively; (c) $P_d$ $(\alpha_c=0.3)$ are $6.40\times10^{-2}$, 0.141, 0.252, 0.511, and 0.761 for $\tau=10$ fs, 50 fs, 100 fs, 250 fs, and 500 fs, respectively; (d) $P_d$ $(\alpha_c=0.3)$ are 0.106, 0.259, 0.435, 0.765, and 0.940 for $\tau=$ 10 fs, 50 fs, 100 fs, 250 fs, and 500 fs, respectively.

downward such that the resonant frequency $V_2-V_1$ decreases with time. For the case of a positively chirped pulse, the pulse becomes off resonant with the moving wave packet before the Rabi oscillation starts to deexcite the population back to the ground surface, and can only pump more amplitude up to the excited state. In contrast, the negative chirping can follow the motion of the wave packet and hence cycle the population back to the ground surface. Also, the data show that the transition probability is proportional to the pulse duration at this field intensity. This is the typical Fermi golden rule characteristics in the perturbation regime.

Figure 2(b) shows results at a field intensity 100 TW/cm$^2$. The behavior is again perturbative except in the case of a 10-fs pulse. In our previous study [14], we showed that population inversion is determined by the adiabatic criterion $|d\omega_L/dt|\ll|E(t)\mu(R)|^2$, therefore the longer pulse duration implies the slower frequency sweeping in Fig. 3, hence the longer duration pulse is more efficient than the shorter duration pulse in excitation. Due to the fast frequency sweeping rate of the shortest pulse, the 10-fs case is the first to go beyond the adiabatic approximation and behaves differently from the other cases. As the field intensity increases further

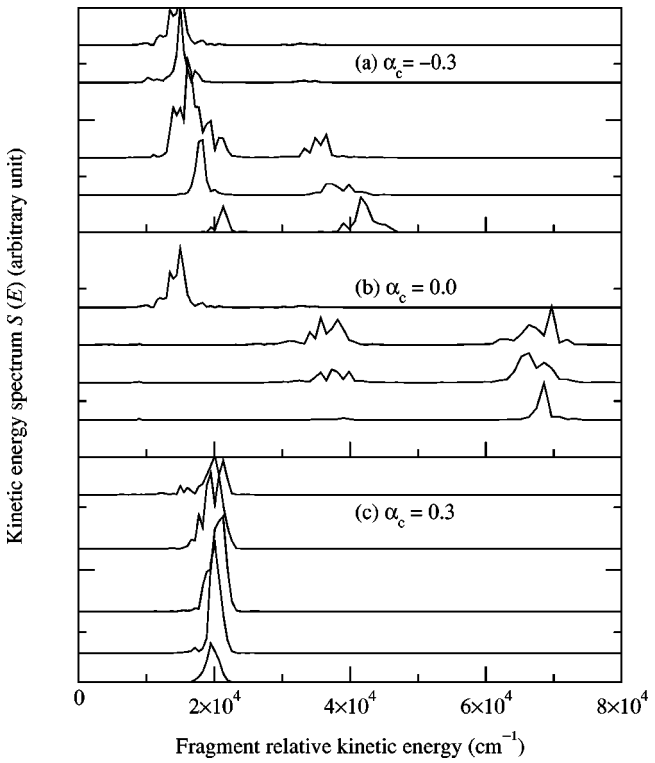


FIG. 3. Proton kinetic-energy spectra (PKES) of pulse duration 500 fs, with various chirping. In each plot, the intensities from bottom to top for each PKES are $1\times10^{12}$ W/cm$^2$, $5\times10^{12}$ W/cm$^2$, $3\times10^{13}$ W/cm$^2$, $8.75\times10^{13}$ W/cm$^2$, and $1\times10^{14}$ W/cm$^2$, respectively. All the PKES have been enlarged such that there is no absolute relation between the peak intensity in this figure. Note also that there is no PKES for $\alpha_c=0.0$ and intensity $I=1\times10^{12}$ W/cm$^2$ in plot (b).

in Figs. 2(c) and 2(d), the criterion difference among all pulse durations of the same chirping parameter $\alpha_c$ is significant, which makes the dissociation probability distinguishable even after scaling. We can also see that there is a slow oscillatory behavior of $P_d$ against $\alpha_c$ in Fig. 2. This could be due to the interference pathways in the dissociation process, as shown in [14,15].

The PKES are depicted in Fig. 3 for five different pulse intensities of duration 500 fs with chirping constant $\alpha_c=-0.3$, 0, and $+0.3$. This PKES describes the kinetic energy of the relative motion of dissociation fragments, proton and hydrogen atom, of $H_2^+$ in the center-of-mass (CM) frame. Therefore, each dissociation fragment shares nearly the same kinetic energy in the asymptotic region, that is, one-half of the relative kinetic energy in the CM frame. Figure 3(b) contains PKES for the $\alpha_c=0$ case with intensity at 1, 5, 30, 87.5, and 100 TW/cm$^2$. From this figure, we can see that there is a negligible dissociation signal at 1 TW/cm$^2$. The three-photon absorption peak appears first at 5 TW/cm$^2$. At 30 TW/cm$^2$, there are two groups of subpeaks corresponding to the three-photon absorption–one-photon emission–3-photon absorption process. At an intensity of 100 TW/cm$^2$, there remains only one group of subpeaks corresponding to the three-photon absorption two-photon emission process. Comparing to Fig. 5 of Ref. [19], we know that the spectral

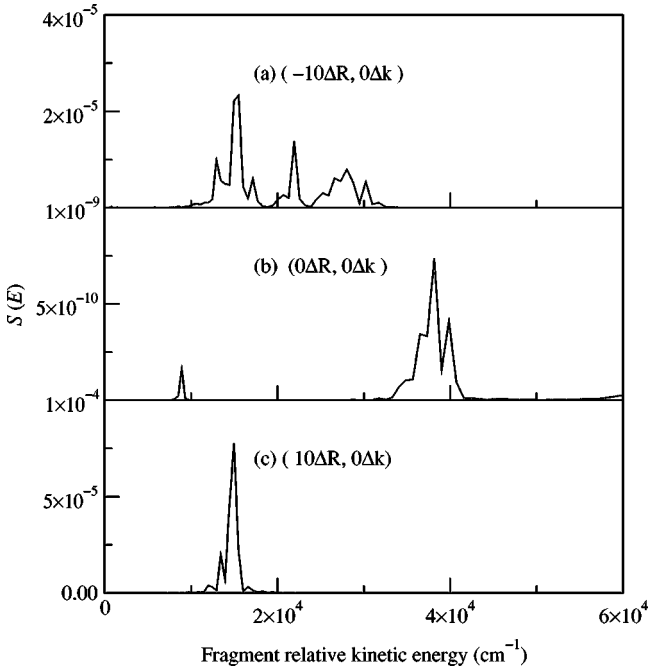


FIG. 4. PKES of different $\langle R \rangle$ shifts at chirping-free pulse intensity $5\times10^{12}$ W/cm$^2$ with duration $\tau=250$ fs. The shifts are in units of $\Delta R$, where $\Delta R$ is 0.0625 a.u. in the present calculation. In (a) the $-10\Delta R$ shift results in a broadened vibrational state distribution up to $v=9$, while $v$ distribution is only at ground state in (b). The distribution in (c) is intermediate between (a) and (b) with populations up to $v=3$. The PKES have been offset from zero in the vertical direction for clarity. In (b), a three-photon absorption peak that is one order of magnitude larger than a two-photon peak is not shown in this plot.

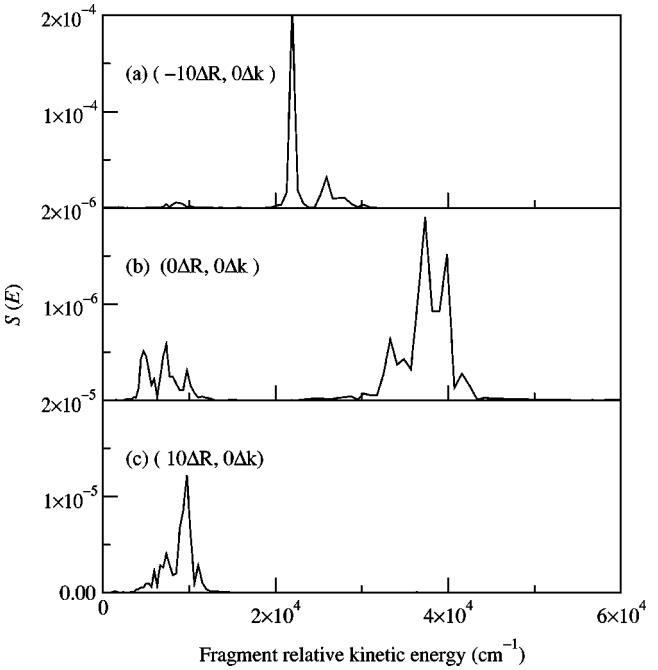


FIG. 5. Same as Fig. 4 except the intensity $I$ is $8.75\times10^{13}$. The three-photon peak not shown here is about one order of magnitude smaller than the two-photon peak in (b).

structure is complicated as field intensity goes above $3\times10^{13}$ W/cm$^2$ with longer pulse duration, such that the wave packet can be excited to and deexcited from the $^2\Sigma_u$ state and produces other excited vibrational components in the $H_2^+$ ground electronic state [5,16]. The results confirm the multiphoton processes against field intensity, as shown in Fig. 1 of Ref. [9].

Besides, the three-photon peaks are well located at $3\omega_L$ as expected and the two-photon peaks are slightly redshifted. This is because the photon-exchange mechanism dominates in the three-photon process for lower intensity without photon emission during the dissociation process, while the two-photon process has one photon emitted when the wave packet moves away from the molecular center. The one-photon peak dominates at high intensity, corresponding to a three-photon mechanism of the absorption-emission-emission process that can also be interpreted as a tunneling through an adiabatic barrier after reflection, resulting in a blueshift in the PKES.

When $H_2^+$ is irradiated by chirped pulses, the PKES are quite different from the chirping-free cases even with the same field intensity. Figure 3(a) are the results of negative chirping. We find that the three-photon absorption peak disappeared and the two-photon (three-photon absorption–one-photon emission) peaks shift from blue to red around $2\omega_L$ as the intensity increases. Similar behavior is observed for the one-photon (three-photon absorption–two-photon emission) peaks. The shifts tell us that the multiphoton processes occur sequentially at a different moment for each intensity, or the photon exchange happens frequently during the excitation process, and the negative chirping causes the redshifts.

On the other hand, there is only one photon peak in the positive chirping PKES, and the peak width and structure increase with intensity. The peak shift is absent in positive chirping, a plausible reason being that there is no more photon exchange after $H_2^+$ absorbs one photon at some moment during the excitation process because it is hard to be deexcited from a $^2\Sigma_u$ state for a positive chirped pulse [16]. Therefore, we know that high-energy PKES could be suppressed by pulse chirping.

Comparing the results above with Figs. 1 and 3 of Ref. [1], we can see that the dynamics studied in this work is not independent of chirping direction as it was in Ref. [1]. The lack of symmetry about the chirping direction in our work may be due to the following reasons. (i) The chirping parameter of Ref. [1], in the bandwidth limit, varies from $-0.09$ to 0.09 therein. In this small range of chirping value, the dynamics does not change significantly and is nearly symmetric in both directions of chirping. In our case, the chirping parameter changes from $-0.3$ to 0.3, about three times larger than 0.09. (ii) In Ref. [1], the intensity is above 100 $TW/\mathrm{cm}^2$, which may be strong enough to saturate the dissociation probability, and has no effect on the positive and negative chirping in the chirping excitation of rubidium [30]. On the other hand, the intensity used in this paper is intermediate and the dissociation probability *does not saturate*. (iii) Since the frequency used in Ref. [1] is 792 nm, well below the dissociation limit, and the PKES is the one-photon peak, there is no reason to deduce the dissociation mecha-

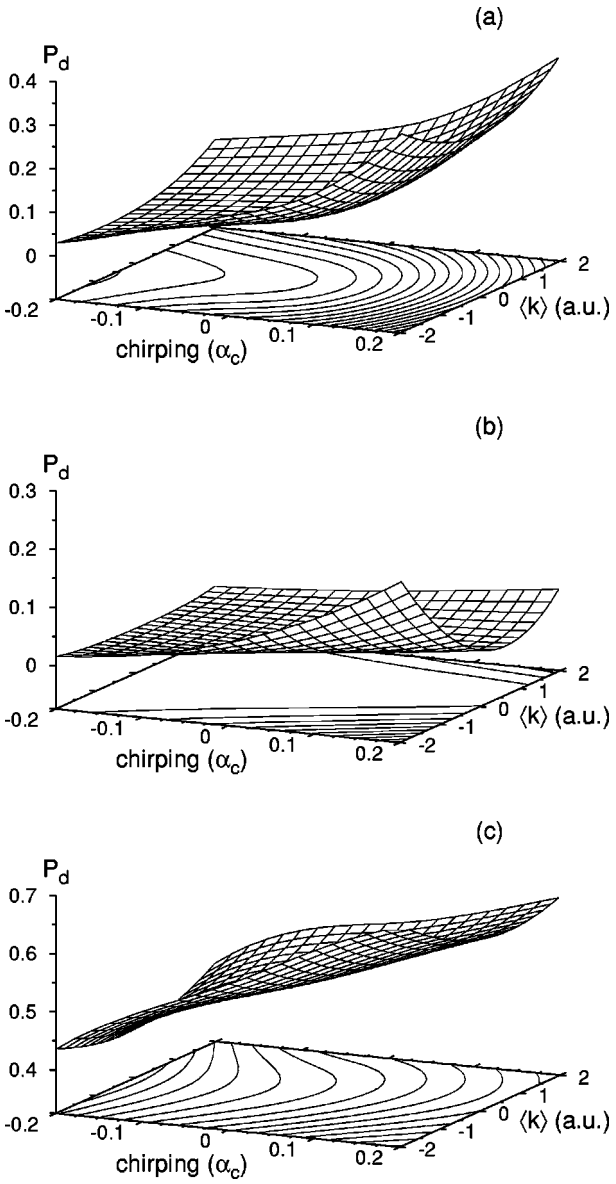


FIG. 6. Dissociation probabilities $P_d$ as functions of $\alpha_c$ and momentum shift $\langle k \rangle$ at $\tau = 10$ fs and $I = 8.75 \times 10^{13}$ W/cm$^2$. From top to bottom, the spatial shift $\langle R \rangle$ is $8\Delta R$, $0\Delta R$, and $-8\Delta R$ in each plot, respectively. The contour level increased by a step of 0.02.

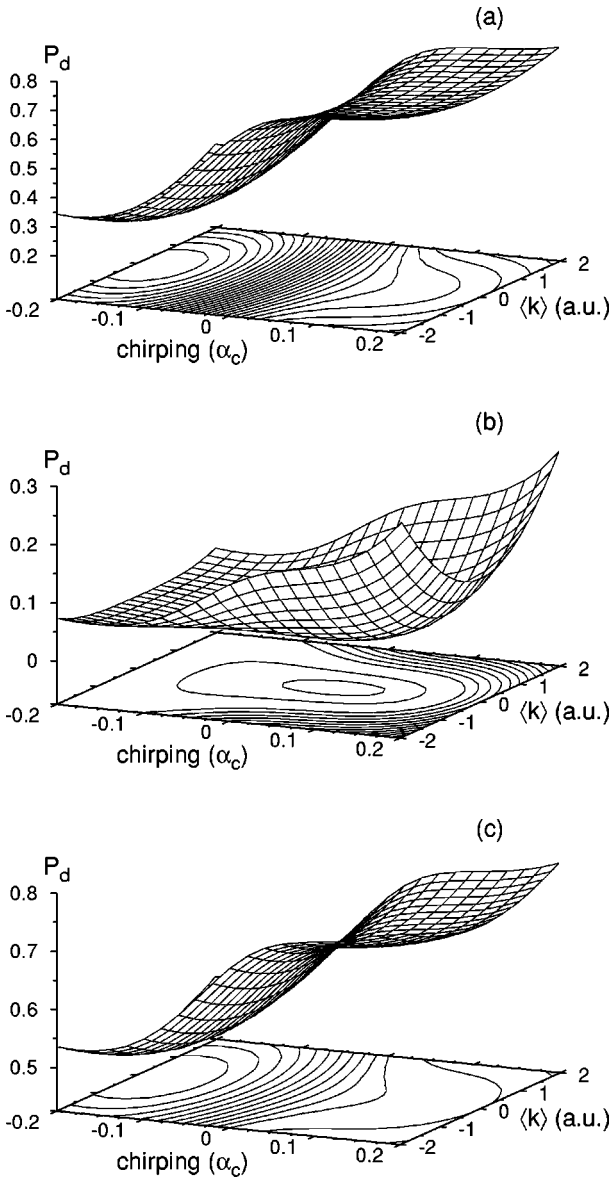


FIG. 7. Same as Fig. 6 except pulse duration $\tau = 250$ fs.

nism dominated by the multiphoton process. Instead, the tunneling process becomes the only possibility in contrast to the 330 nm, which is a little larger than the dissociation threshold. The initial states starting at $v = 3$ and 4 also enchance the tunneling dissociation for the intense field 100–200 TW/cm$^2$. The strong peak field and small frequency prefer this diabatic (tunneling) dissociation mechanism rather than the adiabatic passage (multiphoton) process because the Keldysh parameter $\gamma$ ($\propto \omega_0 / E_m$) is smaller and the adiabatic passage criterion $[|d\omega_L/dt| \ll |E(t)\mu(R)|^2]$ is more unsatisfied in Ref. [1] than in this paper. To sum up, the main difference between Ref. [1] and our results is the intensity, pulse frequency, and chirping parameter.

In Figs. 4 and 5, we show the PKES of initial states with the same shape but shifted to a different position $\langle R \rangle$ for $I = 5 \times 10^{12}$ W/cm$^2$ and $8.75 \times 10^{13}$ W/cm$^2$, respectively. The pulse duration $\tau$ is 250 fs and $\alpha_c = 0$ in both figures. In Fig. 4(b), the inset shows that the initial wave packet contains only the vibrational ground state of $H_2^+$ $^2\Sigma_g$, while the distribution in Fig. 4(c) is up to $v = 3$ and it extends to $v = 9$ in Fig. 4(a). The vibrational energy difference of $v = 1$ and $v = 0$, $\Delta E_{1,0}$, is 2239 cm$^{-1}$ and decreases stepwise 6% for neighboring states to $\Delta E_{9,8} = 1247$ cm$^{-1}$. Therefore, at weaker intensity there is a blueshift one-photon peak that broadens about $2 \times 10^4$ cm$^{-1}$ to include $H_2^+$ ten vibrational levels in Fig. 4(a), and the vibrational distributions of Figs. 4(b) and 4(c) are reflected by the one-photon peaks that result from the absorption of one photon without emission, while the structure of the subpeaks corresponds to the two-photon peak coming from the absorption-emission process.

As the intensity increases, the one-photon PKES may result from the tunneling of high vibrational levels or photon exchange, i.e., absorption of three photons and emission of

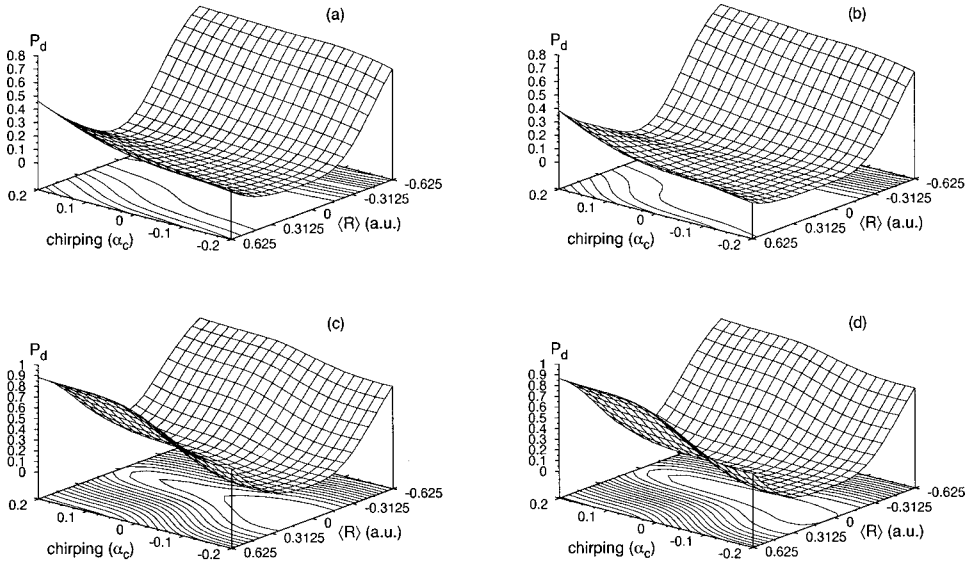


FIG. 8. $P_d$ vs $\alpha_c$ and $\langle R\rangle$ at $I=8.75\times10^{13}$. (a) $\tau=10$ fs and $\langle k\rangle=8\Delta P$; (b) $\tau=10$ fs and $\langle k\rangle=0$; (c) $\tau=250$ fs and $\langle k\rangle=8\Delta P$; (d) $\tau=250$ fs and $\langle k\rangle=0$. The contour level is increased by a step of 0.02.

two photons of lower vibrational levels. In Fig. 5(a), the high vibrational state tunneling dominates in the PKES because the vibrational distribution is up to $v=9$ and the multiphoton absorption signal of low vibrational levels is about one or two orders of magnitude smaller than the tunneling PKES. In contrast to Fig. 5(a), the PKES in Fig. 5(b) is located around the one-, two-, and three-photon position due to its distribution being only on $v=0$, which is below the potential barrier formed by the potential curve and the laser field. Figure 5(c) has a vibrational distribution between $v=0$ and 3 resulting in PKES of one-photon absorption at about $1\times10^4$ cm$^{-1}$. The results of Figs. 4 and 5 can be summarized as follows: for weaker field, the dominant process is via photon absorption, especially for the one-photon peak without any photon emission. On the other hand, tunneling or absorption-emission becomes important in the strong field regime. It is evident by comparing Figs. 4(a) and 5(a) that there is a sharp peak in Fig. 5(a) and those subpeaks appearing in Fig. 4(a) almost disappear in Fig. 5(a).

The dissociation probabilities $P_d$ as a function of chirping parameter $\alpha_c$ and the initial wave function's shifted coordinates are shown in Figs. 6–9 with a pulse intensity of $8.75\times10^{13}$ W/cm$^2$ at various pulse durations. The dissociation probabilities are nearly symmetric about $\langle k\rangle=0$ in each plot and increase as $|\langle k\rangle|$ increases in Figs. 6 and 7. This is possibly due to the short vibrational period of the wave packet such that the pulse duration could cover many vibrational periods when the wave packet moves in the ground potential surface. Therefore, the excitation relation between the wave-packet motion and the chirping direction is averaged out and we have to use an ultrashort chirped pulse to explore this short time dynamics whenever we want to observe this relation. For $\langle R\rangle\neq0$, it seems that dissociation probabilities increase with positive $\alpha_c$ and decrease at negative chirping parameter, but they do not have the similar behavior of Figs. 6(b) and 7(b). In addition, the features of the dissociation probabilities $P_d$ are different in Figs. 6(a) and 6(c) for a short pulse duration of 10 fs, but they look very similar in Figs.

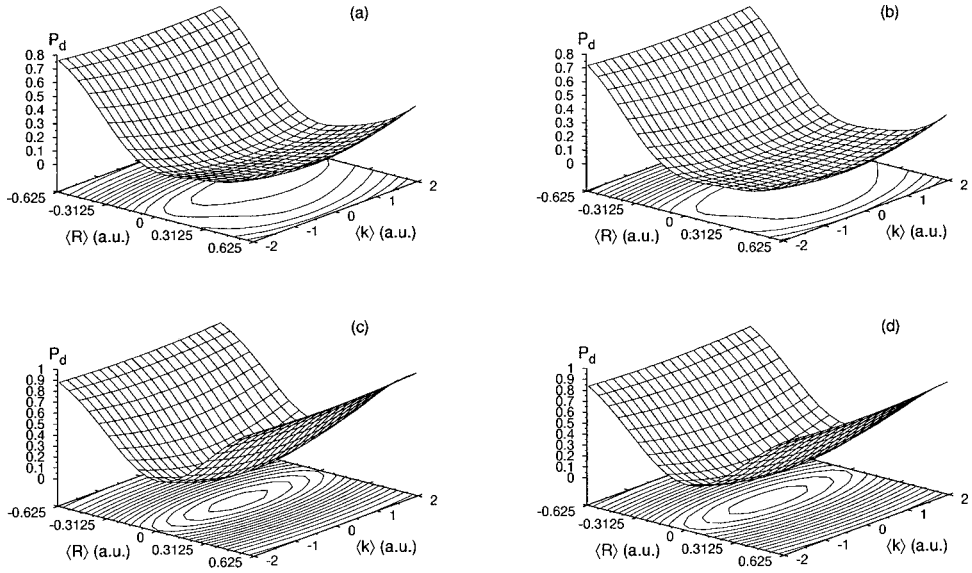


FIG. 9. $P_d$ as a function of $\langle R\rangle$ and $\langle k\rangle$ for different pulse durations and chirping parameters. (a) $\alpha_c=0.1$, $\tau=10$ fs; (b) $\alpha_c=0.0$, $\tau=10$ fs; (c) $\alpha_c=0.1$, $\tau=250$ fs; (d) $\alpha_c=0.0$, $\tau=250$ fs. The contour level is increased by a step of 0.02.

7(a) and 7(c). Figure 8 is the $P_d$ as a function of $\alpha_c$ and $\langle R \rangle$, from which we can see that $H_2^+$ has a large dissociation at negative shift $\langle R \rangle$ and positive chirping $\alpha_c$. As the pulse duration increases, the positive $\langle R \rangle$ shift increases $P_d$ significantly and the dissociation of negative $\langle R \rangle$ does not change much. Finally, Fig. 9 shows that the dissociation probability depends weakly on the $\langle k \rangle$ shift, and an increased pulse duration will increase $P_d$, too.

Thus, we can infer the following. (i) For short pulse duration, the effect of increasing $P_d$ by the $\langle k \rangle$ shift is weak. Positive chirping and $\langle R \rangle$ shift are more able to achieve dissociation than negative chirping. (ii) The dissociation probability of the positive $\langle R \rangle$ shift can be changed drastically by applying a long pulse laser, but the negative $\langle R \rangle$ shift $P_d$ is not able to do that due to its saturation at short pulse duration.

## IV. CONCLUSION

We have shown the possibility of combining a split operator, the generalized Pauli matrix, and splitting wave methods to the time-dependent quantum-mechanical calculation of $H_2^+$ in an intense laser field. This approach is very useful for an intense external field with general field frequency and pulse shape. The higher-energy peaks of PKES with the absorption of many photons would be suppressed by the chirped pulse compared to the chirping-free cases. Besides, the dissociation probability will increase by about one order of magnitude more for the chirping excitation than for the chirping-free one, and positive chirping is more efficient than negative chirping. By slightly shifting the initial state position and/or momentum, the dissociation probability increases prominently with a chirped pulse.

However, because the frequency is sweeping in time, it is difficult to analyze the matter-field interaction via the simple photon-exchange mechanism. In addition, the excitation-deexcitation process is be complicated and more significant as the pulse duration becomes longer (250–500 fs) than for the ultrashort pulse (10–20 fs). Therefore, we propose a plausible way to combine the three methods mentioned above to calculate the transition between multipotential surfaces of molecules and to explore the dissociation dynamics including the dissociation probability and PKES. Detailed dissociation dynamics and extension to three-dimensional systems with an intraband rovibrational transition and excitation control will be investigated in future works.

## ACKNOWLEDGMENTS

The authors acknowledge the National Science Council of Taiwan for financial support under Contract No. NSC89-2112-M009-044. One of us (J.T.L) is partially supported by the Computational Materials Research Program, NCTS, Taiwan.

[1] L. J. Frasinski, J. H. Posthumus, J. Plumridge, and K. Colding, Phys. Rev. Lett. **83**, 3625 (1999).
[2] T. J. McIlrath, P. H. Bucksbaum, R. R. Freeman, and M. Bashkansky, Phys. Rev. A **35**, 4611 (1987); J. W. J. Verschuur, L. D. Noordam, and H. B. van Linden van den Heuvell, *ibid.* **40**, 4383 (1989).
[3] A. Giusti-Suzor, H. He, O. Atabek, and F. H. Mies, Phys. Rev. Lett. **64**, 515 (1990).
[4] P. H. Bucksbaum, A. Zavriyev, H. G. Muller, and D. W. Schumacher, Phys. Rev. Lett. **64**, 1883 (1990).
[5] A. Zavriyev, P. H. Bucksbaum, H. G. Muller, and D. W. Schumacher, Phys. Rev. A **42**, 5500 (1990).
[6] A. Zavriyev, P. H. Bucksbaum, J. Squier, and F. Saline, Phys. Rev. Lett. **70**, 1077 (1993).
[7] E. Charron, A. Giusti-Suzor, and F. H. Mies, Phys. Rev. Lett. **71**, 692 (1993).
[8] E. E. Aubanel, J. M. Gauthier, and A. D. Bandrauk, Phys. Rev. A **48**, 2145 (1993).
[9] M. Chrysos, O. Atabek, and R. Lefebvre, Phys. Rev. A **48**, 3855 (1993).
[10] O. Atabek and G. Jolicard, Phys. Rev. A **49**, 1186 (1994).
[11] R. Numico, A. Keller, and O. Atabek, Phys. Rev. A **56**, 772 (1997).
[12] G. N. Gibson, M. Li, C. Guo, and J. Neira, Phys. Rev. Lett. **79**, 2022 (1997).
[13] S. Chelkowski, A. D. Bandrauk, and P. B. Corkum, Phys. Rev. Lett. **65**, 2355 (1990); S. Chelkowski and A. D. Bandrauk, J. Raman Spectrosc. **28**, 459 (1997).
[14] J. T. Lin, T. L. Lai, D. S. Chuu, and T. F. Jiang, J. Phys. B **31**, L117 (1998); J. T. Lin and T. F. Jiang, *ibid.* **32**, 4001 (1999); J. T. Lin, M. Hayashi, S. H. Lin, and T. F. Jiang, Phys. Rev. A **60**, 3911 (1999).
[15] B. Broes, H. B. van Linden, and L. D. Noordam, Phys. Rev. Lett. **69**, 2062 (1992); D. J. Maas, D. I. Duncan, A. F. G. van der Meer, W. J. van der Zande, and L. D. Noordam, Chem. Phys. Lett. **270**, 45 (1997); D. J. Maas, D. I. Duncan, R. B. Vrijen, W. J. van der Zande, and L. D. Noordam, *ibid.* **290**, 75 (1998); D. J. Maas, M. J. J. Vrakking, and L. D. Noordam, Phys. Rev. A **60**, 1351 (1999).
[16] J. Cao, C. J. Bardeen, and K. R. Wilson, Phys. Rev. Lett. **80**, 1406 (1998).
[17] S. Meyer, C. Meier, and V. Engel, J. Chem. Phys. **108**, 7631 (1998).
[18] R. Heather and H. Metiu, J. Chem. Phys. **86**, 5009 (1987).
[19] A. Keller, Phys. Rev. A **52**, 1450 (1995).
[20] P. Gross, D. Neuhauser, and H. Rabitz, J. Chem. Phys. **96**, 2834 (1992); E. Charron, A. Giusti-Suzor, and F. H. Meis, *ibid.* **103**, 7359 (1995); K. Mishima and K. Yamashita, *ibid.* **109**, 1801 (1998).
[21] M. D. Feit, J. A. Fleck, Jr., and A. Steiger, J. Comput. Phys. **47**, 412 (1982).
[22] M. R. Hermann and J. A. Fleck, Jr., Phys. Rev. A **38**, 6000 (1988).
[23] L. V. Keldysh, Zh. Éksp. Teor. Fiz. **47**, 1945 (1964) [Sov. Phys. JETP **20**, 1307 (1965)].
[24] M. V. Fedorov, *Atomic and Free Electrons in a Strong Light*

*Field* (World Scientific, Singapore, 1997).
[25] P. Balling, D. J. Mass, and L. D. Noordam, Phys. Rev. A **50**, 4276 (1994).
[26] S. Backus, C. G. Durfee III, M. M. Murnane, and H. C. Kapteyn, Rev. Sci. Instrum. **69**, 1207 (1998).
[27] J. Zhou, J. Peatross, M. M. Murnane, H. C. Kapteyn, and I. P. Christov, Phys. Rev. Lett. **76**, 752 (1996).
[28] C. Spielmann, N. H. Burnett, S. Sartania, R. Koppitsch, M. Schnürer, C. Kan, M. Lenzner, P. Wobrauschek, and F. Krausz, Science **278**, 661 (1997).
[29] D. R. Bates, J. Chem. Phys. **19**, 1122 (1951).
[30] D. J. Maas, C. W. Rella, P. Antoine, E. S. Toma, and L. D. Noordam, Phys. Rev. A **59**, 1374 (1999).